

Optimizing MRI sequences and images for MRI-based stereotactic radiosurgery treatment planning

Somayeh Taghizadeh, MS^{1,2,4}; Cecille Labuda, Ph.D.⁴; Claus Chunli Yang, Ph.D.¹; Bart Morris, MS¹; Madhava R. Kanakamedala, M.D.¹; Srinivasan Vijayakumar, M.D.¹; Roberto Rey-Dios, M.D.^{1,3}; William N. Duggar, M.S.¹; Edward Florez, Ph.D.²; Ali Fatemi, Ph.D.^{1,2}

¹ Department of Radiation Oncology, University of Mississippi Medical Center, Jackson, MS, USA

² Department of Radiology, University of Mississippi Medical Center, Jackson, MS, USA

³ Department of Neurosurgery, University of Mississippi Medical Center, Jackson, MS, USA

⁴ National Center for Physical Acoustics and Department of Physics and Astronomy, University of Mississippi, Jackson, MS, USA

Abstract

Aim

Development of MRI sequences and processing methods for the production of images appropriate for direct use in stereotactic radiosurgery (SRS) treatment planning.

Background

MRI is useful in SRS treatment planning, especially for patients with brain lesions or anatomical targets that are poorly distinguished by CT, but its use requires further refinement. This methodology seeks to optimize MRI sequences to generate distortion-free and clinically relevant MR images for MRI-only SRS treatment planning.

Materials and methods

We used commercially available SRS MRI-guided radiotherapy phantoms and eight patients to optimize sequences for patient imaging. Workflow involved choice of correct MRI sequence(s), optimization of the sequence parameters, evaluation of image quality

(artifact free and clinically relevant), measurement of geometrical distortion, and evaluation of the accuracy of our offline correction algorithm.

Results

CT images showed a maximum deviation of 1.3 mm and minimum deviation of 0.4 mm from true fiducial position for SRS coordinate definition. Interestingly, uncorrected MR images showed maximum deviation of 1.2 mm and minimum of 0.4 mm, comparable to CT images used for SRS coordinate definition. After geometrical correction, we observed a maximum deviation of 1.1 mm and minimum deviation of only 0.3 mm.

Conclusion

Our optimized MRI pulse sequences and image correction technique show promising results; MR images produced under these conditions are appropriate for direct use in SRS treatment planning.

Introduction

Magnetic resonance imaging (MRI) is the imaging modality of choice for target definition for stereotactic radiotherapy due to its superior soft tissue resolution, not only in the brain but in extracranial sites as well. In cases of intracranial stereotactic radiotherapy, MRI can also be used for dosimetry planning as the brain is considered homogenous. The advantages of using MRI alone¹ in intracranial SRS include avoiding systematic errors that may occur due to CT-MRI

registration, and the risks associated with ionizing radiation exposure from CT scans.

Although MR images have excellent soft-tissue contrast, allowing superior visualization of gross tumor volume

.....
The concepts and information presented in this paper are based on research and are not commercially available.

¹ The product is not commercially available. Radiotherapy where MR data is the only imaging information is ongoing research. The concepts and information presented in this article are based on research and are not commercially available. Its future availability cannot be ensured. Not for clinical use.

(GTV) and organs at risk (OAR), the geometrical distortion of MR images is one of the main obstacles to their optimal use in SRS planning; therefore, CT is still commonly used to obtain geometrically accurate reference images. CT images also provide electron density data and can be registered with MR images for geometrical distortion correction [1].

One motivation for the solo use of MRI for SRS planning is most centers' use of Tissue Maximum Ratio (TMR) tables for SRS treatment planning; these tables do not account for brain tissue inhomogeneity. This technique is faster, simpler, and no information about tissue electron density is required; however, many groups are working on synthetic CT images which make use of MR images.

With the use of synthetic CT images derived from MR images, we still retain the option to use convolution/superposition algorithms in SRS treatment planning for more accurate dose calculation.

The geometrical accuracy of MR images can be compromised by both system- and patient-specific distortions. System related distortion is mainly caused by main magnetic field (B_0) inhomogeneity and gradient nonlinearity. These effects are reproducible for each scanner, but vary for different field strengths and vendors, and must be evaluated during the commissioning process. [2]

The B_0 of an MRI is measured in parts per million (ppm) over a diameter of spherical volume (DSV) extending out from the scanner isocenter. We expect a nominal homogeneity of 1.1 ppm across a 37 cm DSV for a 1.5T scanner; this corresponds to a frequency offset of 70.2 Hz. This offset resonance frequency along the frequency encoding direction creates discrepancies in signal location which manifest as image intensity variation and distortion.

Gradient coils localize the MRI signal within the body to visualize the anatomy. Many newly developed fast MRI pulse sequences have been used in the clinic to minimize artifacts due to motion and provide patient comfort. These sequences need strong gradients, but there is always a tradeoff between gradient strength and linearity. The gradient linearity error should be less than 2% of the gradient strength over a 40 cm diameter of spherical volume (DSV) [3].

Modern MRI scanners have homogenous magnetic fields; therefore, the main source of image distortion is gradient non-linearity. Most vendors provide post-processing offline correction algorithms, which are applied in two and three dimensions [4–6], but still there is a need to evaluate the efficiency of such corrections with periodic phantom measurements.

Patient-specific distortion originates from the effect of tissue magnetic susceptibility (χ) on the local magnetic field. These random distortions are not corrected by standard MRI post-processing correction algorithms and need careful consideration, especially when MR images are being used as a sole source for SRS planning. Patient-specific distortion may cause tumor and normal tissue dislocation, significant error in stereotactic coordinates definition, and MRI-CT co-registration difficulty, especially when targets in the brain are very close to air cavities, or away from the magnet isocenter.

Several methods have been suggested to correct patient-specific distortion. One is an increase in receiver bandwidth, but increasing the bandwidth leads to a reduction in the signal-to-noise ratio (SNR) [7, 8]. Another is to use manual and high-order shimming to render the magnetic field more locally homogenous by minimizing the effect of magnetic susceptibility, chemical shift and eddy current through the region of scan [9–11]. Finally, a B_0 field map, very commonly used in functional MRI (fMRI) studies, has been used to correct for geometrical distortions in echo planar imaging (EPI) images [12]. All of these methods have their own advantages and disadvantages, but for our purposes, to be used in the SRS clinic, their accuracy, clinical flow, and compatibility with SRS treatment planning system are vital factors [12].

Different MRI sequences (different contrasts) are being used for GTV and OAR contouring in SRS treatment planning systems. Depending on the clinical protocol implemented, CT and MRI images may initially define the stereotactic coordinates, and then CT image set is co-register rigidly to MR images to correct for any noticeable geometrical distortion. Importantly, to accurately correct MR images they must be registered deformably not rigidly with CT images which is not an option with the current SRS Gamma Knife treatment planning systems. Specifically, distortions are more noticeable when MR images are collected in 2D mode, with different slice thickness, in-plane or through-plane spatial resolution compared with CT, and in partial head scans in oblique mode.

In this paper, we describe our methodology to generate distortion-free and clinically relevant MR images for MRI-only SRS treatment planning. We tested our method first on commercial phantoms, and then on patients. Our methodology involves choosing the right MRI sequences, optimizing the sequence parameters, evaluating the image quality, determination of clinical relevance, correction for geometrical distortion, and finally, testing the accuracy of our offline correction algorithm.

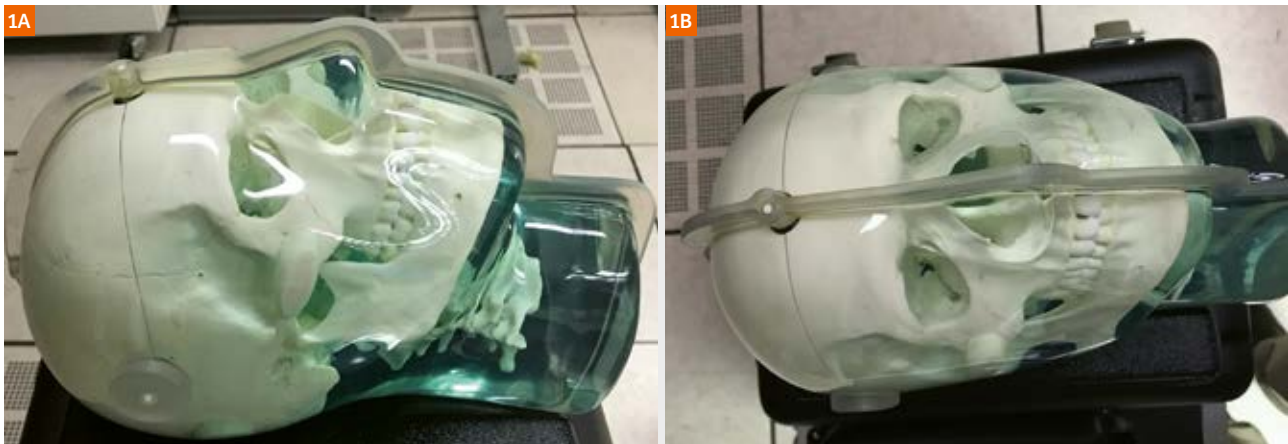


Figure 1:
CIRS Simulated MRI distortion head phantom.

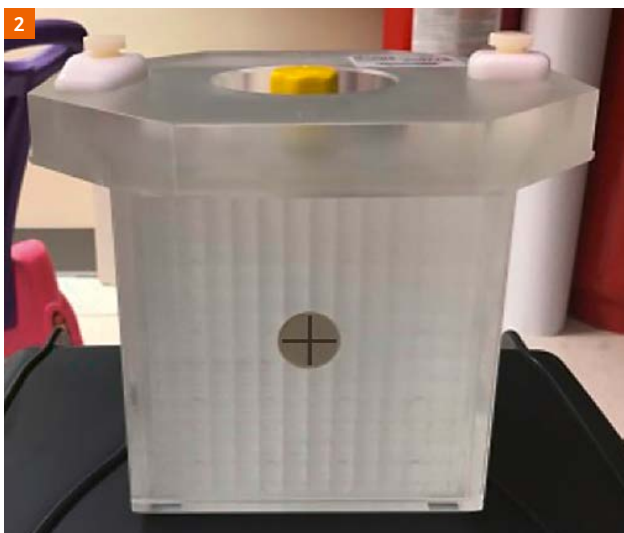


Figure 2:
Quasar GRID^{3D} image distortion phantom: "small phantom".

Materials and methods

We have recently installed the new Leksell Gamma Knife[®] Icon™ stereotactic radiosurgery treatment unit² (Elekta AB, Stockholm, Sweden), and the MAGNETOM Aera 1.5T Radiotherapy (RT) edition (Siemens Healthcare, Erlangen, Germany) at our institute. The SRS committee consists of three physicists, one radiologist, two radiation oncologists, and one neurosurgeon; together, it is responsible for choosing the clinically relevant MRI pulse sequences for SRS treatment planning.

MR images are used for treatment of brain metastasis, pituitary/parasellar lesions, acoustic neuroma, trigeminal neuralgia, and arteriovenous malformation (AVM). The SRS committee look at specific MRI pulse sequences with unique contrast and resolution to be used for GTV and OAR contouring in a SRS treatment planning system (Gamma Plan, Version 11.0.3). Generally, the MRI sequences are mostly 3D, no slice gap for 2D sequences, and isotropic in spatial resolution. Immobilization devices are chosen to be MRI-compatible based on vendor report and the reports of other centers. Most importantly, the committee chooses the optimal head RF coil(s) for high sensitivity, better SNR, less RF deposition (SAR effect), and retention of enough space to fit the SRS frame, MRI localizer, and RF head adaptor into the scanner.

We initially optimized MRI sequences to have high SNR and provide artifact-free images and then focused on correcting geometric distortion using two commercially available MRI compatible phantoms: a simulated head phantom (CIRS, MRI distortion phantom, Model 603A, Norfolk, VA, USA) (Fig. 1), and a Quasar GRID^{3D} (Modus Medical, London, ON, Canada) (Fig. 2). We then collected data from six SRS patients.

The MRI scanner was commissioned based on our proposed quality control procedure for SRS treatment planning using commercial and standard phantoms. As part of our commissioning process, we evaluated a system distortion map (B_0 inhomogeneity and gradient non-linearity) over a large field-of-view (37 cm) using body coil and Quasar MRID^{3D} (Modus medical, London, ON, Canada) geometrical distortion phantoms (Fig. 3).

We applied system- and patient-specific distortion correction along the frequency encoding direction. The system distortion map was derived using Quasar GRID^{3D}

² The information shown herein refers to products of 3rd party manufacturer's and thus are in their regulatory responsibility. Please contact the 3rd party manufacturer for further information.



Figure 3: Quasar MRID^{3D} geometrical distortion phantom: “big phantom”.

Sequence/contrast	Parameters	Disease
Axial 3D T1-weighted MPRAGE	< 1 mm ³ , TR/TE = 2200/2.91 ms, FA = 15°, 300 Hz/pixel	Brain metastasis, pituitary/parasellar lesions, acoustic neuroma/schwannoma, trigeminal neuralgia, AVM
Axial 3D T2-weighted SPACE	0.9 x 0.9 x 1 mm ³ , TR/TE = 1400/184 ms, FA = 120°, 345 Hz/pixel	Pituitary/parasellar lesions, acoustic neuroma/schwannoma, AVM
Axial 2D T2 TSE	0.9 x 0.9 x 1 mm ³ , TR/TE = 3990/89 ms, FA = 120°, 300 Hz/pixel	Pituitary/parasellar lesions, acoustic neuroma/schwannoma, trigeminal neuralgia

Table 1: MRI pulse sequences used in the phantom studies.

software and our in-house MATLAB code to obtain the “system displacement map”. For patient-specific correction we used a field map technique using a multi-echo Gradient echo sequence to calculate the complex phase difference map with receiver bandwidth and isotropic resolution, close to other MRI sequences.

Phantom study

We scanned the commercial phantoms with SRS frames and localizers on our MRI unit and evaluated the quality of the acquired MR images for artifacts and geometrical fidelity for the purpose of SRS planning. Geometrical distortion was evaluated for different MRI sequences using the GRID^{3D} phantom, and our offline geometrical distortion correction method was validated using phantoms both qualitatively and quantitatively. The GRID^{3D} MRI was scanned with all sequences and parameters summarized in Table 1. All MRI sequences were run with automated shimming over entire phantoms. The central frequency was adjusted manually, and the shimming currents set to apply the highest linear gradient field to each imaging axis. The bandwidths were chosen to be close to 330 Hz/pixel for all MRI sequences to minimize artifacts due to magnetic susceptibility and sub-optimal shimming.

Next, high-resolution magnitude and phase images were acquired to reconstruct the field maps after automated shimming over the entire head phantom volume (Multi-echo gradient echo, TE₁/TE₂/TR = 2.46/11.98/12 ms, 335 Hz/pixels, approximately 1 mm³ isotropic sagittal, 3D acquisition, Rx/Tx RF head coil). The phase images were complex divided and unwrapped to produce field maps (in-house software, IDL 8.2, Boulder, CO, USA and Mathworks, Natick, MA, USA). The conversion of field map to displacement map was found using

$$d = \Delta\chi \cdot f_0 \cdot \frac{\left(\frac{b}{B_0}\right)}{\Delta f}$$

where $\Delta\chi$ is the pixel size, f is the Larmor frequency, Δf is the receiver bandwidth per pixel, B_0 is the magnetic field, and b is the magnetic distortion. The final displacement map was calculated based on the field map and machine displacement maps. The machine displacement map applied to all MRI images in all directions, and the field map applied only in the frequency encoding direction.

For this procedure to be consistent, MR images and displacement map should have the same spatial resolution

and pixel bandwidth, which was checked using an open-source AFNI software package. The region of interest measures $14 \times 13 \times 11 \text{ cm}^3$, and within it are 2002 vertex locations, the positions of which are known within 0.1 mm. The phantom accurately and reproducibly mounts securely to the Leksell Coordinate SRS Frame G at a known position, and fits within both the Leksell MR and CT boxes.



Figure 4: CIRS head phantom with SRS frame and all localizer devices.

We evaluated geometrical distortion for each sequence using the phantom vendor's software. The software automatically finds the fiducials and locates each vertex within the phantom in 3D. The software determined the X, Y, Z, and dr (absolute distance from isocenter) deviations of the location of each vertex in the image. There after we corrected all the MR images using our offline correction and compare with non-corrected images.

Next, the CIRS phantom with SRS frame and localizer (Fig. 4) was scanned by MRI pulse sequences with parameters listed in (Table 1) and by CT (Siemens Healthcare, 120 kV, 462 mA, $512 \times 512 \times 306 \text{ mm}^3$, exposure time 615 ms).

We used MIM software (MIM software Inc., Cleveland, OH, USA) to evaluate MR corrected image quality for artifacts and geometrical accuracy compared with CT. The corrected MR images were rigidly fused with CT (Fig. 5). The geometrical accuracy of the corrected and non-corrected MR images was evaluated visually (checker board) and quantitatively by looking at the fusion matrix statistical parameters such as normalized mutual information (NMI), Pearson correlation coefficient (PCC) and root mean square difference (RMSD).

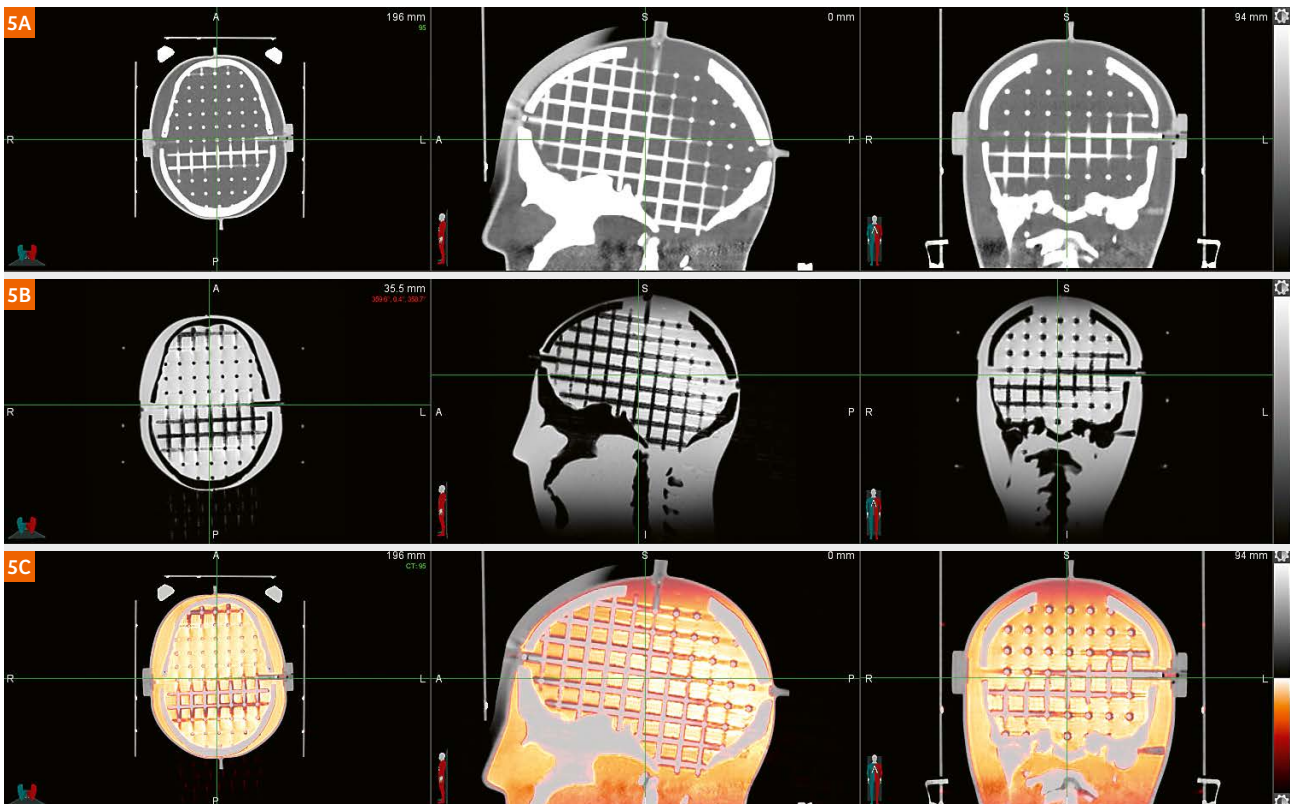


Figure 5: Phantom corrected MRI images fused with CT images. (5A) CT image, (5B) corrected MRI images, (5C) fused MRI and CT images.

Patient study

Eight patients (four with a SRS frame and four with a mask) under an IRB-approved protocol were MRI and CT scanned for SRS treatment. For all patients, we used a 3D post-contrast axial MPRAGE MRI pulse sequence for stereotactic coordinate definition and tumor delineation because of its geometrical accuracy and high SNR. The other MRI sequence has been used for organ at risk (OAR) contouring. The MR images were presented to the radiologist, neurosurgeon and physicist for review of image quality, clinical relevance, and overall scanning time.

The geometrical distortion of MR images before and after correction has been validated qualitatively (checker board) in MIM software with respect to reference CT (Fig. 6). We also imported corrected and non-corrected MR images in GammaPlan and evaluated the stereotactic coordinates definition accuracy relative to CT.

Results

The data from the GRID^{3D} phantom indicate the best MRI geometrical accuracy was obtained with a 3D SPACE sequence. We measured maximum deviation on, (X, Y are

in plane and Z along the magnet), (X-direction = 1.8 mm, Y-direction = 2.9 mm, Z-direction = 2.7 mm) and 0.7 mm on axial plane at 7.5 cm from isocenter in Z direction. We noticed significant artifacts at the boundary, which we speculate were due to magnetic susceptibility from the phantom, SRS frame and localizer. The 3D MPRAGE axial (the reference images) were superior in SNR, and appeared to be less prone to artifacts due to magnetic susceptibility, but showed higher distortion compared to 3D SPACE. We measured maximum deviation (X-direction = 1.9 mm, Y-direction = 2.8 mm, Z-direction = 3.4 mm) and 1.4 mm and 1.3 mm in axial plane beyond 5 cm from isocenter in Z direction. The 2D TSE sequence had an acceptable SNR and was free of artifacts, but as we expected from 2D sequences, the geometrical distortion is extreme, and we do not recommend its use for this application. We measured maximum deviation (X-direction = 2.2 mm, Y-direction = 4.1 mm, Z-direction = 7 mm) and average of 1.8 mm in axial plane beyond 2 cm from isocenter.

After geometrical correction was applied to all images, they were reevaluated. We observed overall improvement in both 3D MPRAGE and 3D SPACE images, but no significant improvement in images obtained using 2D TSE.



Figure 6: Patient corrected MRI images fused with CT images. **(6A)** CT image, **(6B)** corrected MRI images, **(6C)** fused MRI and CT images.

For 3D MPRAGE the changes were minor, and there was improvement in axial plane from 0.8 mm to 0.7 mm for 3 cm and 4 cm from isocenter in Z-direction. 3D SPACE images showed significant improvement; overall 3% correction (average of 0.3 mm) for all points. The TSE images do not show significant improvement which proved that our correction algorithm need to be applied to each slice separately and re-evaluated.

After the MR images from CIRS phantom were reviewed by the SRS committee for image quality, the fusion matrix statistical parameters of fused geometrically corrected and non-corrected MRI and CT images were also examined, and are summarized in Table 2.

The patient MR images were reviewed by the SRS committee for image quality and clinical relevance for SRS treatment planning. All images were geometrically corrected based on the same algorithm used in the phantom studies; we evaluated our patient MRI geometrical accuracy qualitatively (Fig. 6) and quantitatively. First, MIM software was used to rigidly register MR-CT images, visually inspect the checker board display, and calculate the fusion matrix statistics (NMI, PCC and RMSD).

We observed maximum changes of 2% in RMSD for all images and no significant changes in the remaining parameters without significant change. SRS treatment planning software was then used to calculate the stereotactic coordinate accuracy, comparing corrected

MR images to original non-corrected MR images and CT images. The CT images showed the maximum (1.3 mm) and minimum of (0.4 mm) deviation from true fiducial position for SRS coordinate definition. Interestingly the non-corrected MR images showed maximum (1.2 mm) and minimum of (0.4 mm) deviation which is comparable to using CT images for SRS coordinate definition. After geometrical correction we observed the maximum (1.1 mm) and minimum (0.3 mm) deviations.

Discussion

In this work, we demonstrated the methodology and clinical flow to optimize MRI sequences to generate images for MRI only SRS treatment planning. A 3D MPRAGE sequence with high bandwidth generated artifact-free images on both phantoms and patients with acceptable geometrical distortion even prior to offline geometrical correction. Therefore, this sequence is recommended as the main sequence for SRS planning purposes. The 3D axial T2 SPACE has shown significant artifacts in both phantom and patient studies, possibly a result of SRS frame magnetic susceptibility and some wrapping artifacts in the axial plane. In patient studies, we managed to correct for wrapping by putting 60% oversampling in a frequency encoding direction at the expense of increasing scanning time, or using 3D coronal T2 SPACE. Another alternative would be use of a 2D Turbo Spin Echo (TSE) sequence with zero gap.

CIRS Phantom	Non-corrected	Corrected
T1 MPRAGE, BW = 300 Hz/pixel		
Normalized mutual information (NMI)	0.241	0.241
Pearson correlation coefficient (PCC)	0.563	0.565
Root mean square difference (RMSD)	1133.192	1132.724
T2 SPACE, 780 Pixel/Hz, axial		
Normalized mutual information (NMI)	0.171	0.171
Pearson correlation coefficient (PCC)	0.486	0.488
Root mean square difference (RMSD)	824.748	824.719
T2 TSE, axial, BW = 254		
Normalized mutual information (NMI)	0.563	0.563
Pearson correlation coefficient (PCC)	0.563	0.563
Root mean square difference (RMSD)	0.563	0.563

Table 2: The statistical parameters for corrected and non-corrected MRI images fused with CT image.

One of the main obstacles to the direct use of MR images in treatment planning is their geometrical **distortion**¹. In general, SRS treatment planning systems use rigid MRI-CT co-registration, which does not correct for any residual MR image distortion. This correction could be accomplished by using both deformable and rigid co-registration algorithms to create distortion-free MR images if CT images are used as a **reference**³. We propose offline MR images distortion correction be used with SRS treatment planning systems.

Our correction technique is based on communitive effects of system distortion and patient distortion (e.g. head geometry, tissue type, SRS frame material, localizer box). Although most of the literature on MR images distortion correction suggest visual checking, this method does not provide any quantitative information, especially when only a rigid co-registration algorithm is **used**.⁶ Therefore, we proposed two methods to evaluate the MR images distortion quantitatively reporting

1. co-registration accuracy statistics between corrected MR and CT images using, normalized mutual information (NMI), Pearson correlation coefficient (PCC) and root mean square difference (RMSD) and
2. the stereotactic coordinate definition accuracy in SRS treatment planning system for corrected MR images compared with original non-corrected MR and CT images for both phantom and patient studies. We propose to speed up the correction process by using 3D T1 post MPRAGE images as reference, and then registering these images with those acquired using other sequences. These images can then be used for SRS treatment planning.

The two main sources of MRI geometrical distortion (systematic and induced magnetic susceptibility) [12, 13] have been evaluated in a head-sized region by using a commercial MRGRID^{3D} phantom. After applying the vendor's post processing correction for gradient non-linearity, the images' geometrical distortion is within expectations, especially at the central region of magnet (head size), with an average of 0.7 mm – 0.8 mm for 3D SPACE and 3D MPRAGE respectively. To achieve a sub-millimeter accuracy for SRS planning the residual gradient nonlinearity and patient specific distortions (tissue and frame induce magnetic susceptibility) still need to be corrected [14–15].

Patient-specific geometrical distortions have been corrected using a field map technique with the receiver bandwidth close to our MRI pulse sequences to avoid or minimize the inherited distortion in our field maps.

MR images were acquired with high receiver bandwidth, high readout gradient and optimized SNR. Auto shimming was applied for the entire head volume to avoid any distortion due to microscopic gradients, especially if manual shimming was applied for smaller volumes (air cavities and sinuses). There are many studies indicating that susceptibility-induced displacements are most noticeable in **air cavities**¹⁵, and our results from displacement mapping confirmed this statement. Based on our parameters, which we used for SRS MRI sequences (close to 350 Hz/pixel, approximately 1 mm³ isotropic voxels), for axial 3D MPRAGE the maximum displacement was calculated as up to 1.4 mm.

For our next study, we will investigate the geometrical and dosimetric accuracy of MRI-only SRS planning compared to the combined MR/CT image-based planning. There are also opportunities to use corrected MRI-derived CT images (synthetic CT) for MRI-only SRS planning. This opens up the potential to benefit from both soft tissue contrast and inhomogeneity correction using convolution-based dose calculation algorithms for accurate SRS treatment planning accounting for heterogeneity in patient anatomy. Such research projects have implications beyond SRS treatment planning; this methodology could have potential applications in focal brain external beam radiotherapy (IMRT) using synthetic CT images. We strongly believe that the benefits of superior soft tissue contrast from MRI will affect the course of highly conformal image-guided radiotherapy.

Conclusions

In conclusion, our optimized MRI pulse sequences and corrected images show promising results, producing MR images appropriate for direct use for SRS treatment planning. These results highlight the urgency of design and implementation of commercial image processing software compatible with SRS treatment planning systems for MRI distortion correction, and more importantly, multi-modality image registration and post-response tumor evaluation. The commonplace presence of an MRI expert to optimize MRI sequences and establish MRI QA programs in departments of radiation oncology is an inevitable outcome. These findings have implications for SRS planning and MR-guided radiotherapy in general.

Acknowledgments

The authors would like to thank Siemens Healthineers and especially all members of the MRI service crew for fruitful discussions.

References

- 1 Schmidt MA, Payne GS. Radiotherapy planning using MRI. *Phys Med Biol* 2015; 60:R323–61.
- 2 Baldwin LN, Wachowicz K, Thomas SD, Rivest R, Fallone BG. Characterization, prediction, and correction of geometric distortion in 3 T MR images. *Med Phys* 2007; 34:388–99.
- 3 Jezzard P. The physical basis of spatial distortions in magnetic resonance images. In: Bankman IN, editor. *Handbook of medical image processing and analysis*, 2nd ed. Amsterdam: Elsevier; 2009, p. 499–514.
- 4 Walker A, Liney G, Metcalfe P, Holloway L. MRI distortion: considerations for MRI based radiotherapy treatment planning. *Australas Phys Eng Sci Med* 2014; 37:103–13.
- 5 Wang D, Doddrell DM, Cowin G. A novel phantom and method for comprehensive 3-dimensional measurement and correction of geometric distortion in magnetic resonance imaging. *Magn Reson Imaging* 2004; 22:529–42.
- 6 Doran SJ, Charles-Edwards L, Reinsberg SA, Leach MO: A complete distortion correction for MR images: I. gradient warp correction. *Phys Med Biol* 2005; 50:1343–61.
- 7 Reinsberg SA, Doran SJ, Charles-Edwards EM, Leach MO. A complete distortion correction for MR images: II. rectification of static-field inhomogeneities by similarity-based profile mapping. *Phys Med Biol* 2005; 50:2651–61.
- 8 Jezzard P, Balaban RS. Correction for geometric distortion in echo planar images from B0 field variations. *Magn Reson Med* 1995; 34:65–73.
- 9 Reber PJ, Wong EC, Buxton RB, Frank LR. Correction of off resonance related distortion in echo planar imaging using EPI based field maps. *Magn Reson Med* 1998; 39:328–30.
- 10 Robson MD, Gore JC, Constable RT. Measurement of the point spread function in MRI using constant time imaging. *Magn Reson Med* 1997; 38:733–40.
- 11 Zeng H, Constable RT. Image distortion correction in EPI: comparison of field mapping with point spread function mapping. *Magn Reson Med* 2002; 48:137–46.
- 12 Harris R, Wesbey G. Artifacts in magnetic resonance imaging. In Kressel HY editor. *Magnetic Resonance Annual* 1988, New York: Raven Press; 1988, p. 71–112.
- 13 Heilbrun MP: Image-guided stereotactic surgery: Adjunct technical advances. In Wilkins RH, Rengachary SS editors. *Neurosurgery Update II*. New York: McGraw-Hill; 1991, p. 373–78.
- 14 Kondziolka D, Dolan EJ, Tasker RR: Functional stereotactic surgery and stereotactic biopsy using a magnetic resonance imaging directed system: Results and comparisons to CT guidance. *Stereotact Funct Neurosurg* 1990; 54/55:237 (Abstract)
- 15 Matakos A, Balter J, Cao Y. Estimation of geometrically undistorted B0 inhomogeneity maps. *Phys Med Biol* 2014; 59:4945–59.

Contact

Ali Fatemi, Ph.D., MCCPM
Senior physicist, Director of MR Guided
Radiotherapy Lab, Assistant professor
Departments of Radiology and
Radiation Oncology
University of Mississippi Medical Center
2500 North State Street
Jackson, Mississippi 39216
USA
Phone: +1 (601)345-0135
afatemi@umc.edu



MR-integrated workflows in Radiation Therapy for MAGNETOM Systems

We have compiled a series of study protocols and practical tips and tricks for several body sites from experts for both experts and novice users, so that everyone can benefit from each-other.

Download the booklet with tips & tricks
and the .edx and .exar1 files at

www.siemens.com/magnetom-world-rt

Not for distribution in the US

Yael Cui, Ph.D.
University of Michigan, Ann Arbor, USA

Robba Rai, MSc and Gary Liney, Ph.D.
Liverpool and Macarthur Cancer Therapy Centre,
Sydney Institute for Applied Medical Research, Sydney, Australia

Eric Paulson, Ph.D.
Medical College of Wisconsin, Milwaukee, USA

Cynthia Mairand, M.D., FRCS, and David Roberts, M.D., FRCP
Centre hospitalier de l'Université de Montréal, Canada

Maja Soblin, Ph.D.
Sahlgrenska University Hospital, Gothenburg, Sweden

**MR-integrated Workflows
in Radiation Therapy**
for MAGNETOM Systems

siemens.com/magnetom-world-rt

**SIEMENS
Healthineers**